JOURNAL OF CATALYSIS **179,** 203–221 (1998)
ARTICLE NO. CA982213

Cu- and Ag-Modified Cerium Oxide Catalysts for Methane Oxidation

Lj. Kundakovic and M. Flytzani-Stephanopoulos[1]

Department of Chemical Engineering, Tufts University, Medford, Massachusetts 02155

Received January 21, 1998; revised June 24, 1998; accepted June 25, 1998

The catalytic activity of nanocrystalline doped ceria and Cu- and Ag-modified ceria for the complete oxidation of methane was studied in this work. The catalyst structure was studied by X-ray diffraction (XRD) and related to the availability of low-temperature oxygen species. Selected samples were also analyzed by STEM/EDX, HRTEM, and XPS. Temperature-programmed reduction (TPR) by H_2 and CH_4, as well as oxygen chemisorption, measurements were used to characterize the different oxygen species present on the catalyst. La and Zr were used as dopants to modify the crystal size and reduction properties of ceria. Enhanced activity for the complete oxidation of methane is discussed in terms of ceria reducibility, crystal size, and formation of oxygen defects at the surface (extrinsic oxygen vacancies). Addition of transition metal oxides (CuO) or transition metals (Ag) improves the low-temperature oxidation activity of cerium oxide. The interaction of ceria with Ag and CuO is a strong function of the crystal size of ceria. In the presence of the transition metal or metal oxide, a small crystal size of ceria favors the formation of highly reducible oxygen species and enhances the methane oxidation activity.

Key Words: **cerium oxide; crystal size; reducibility; methane oxidation; silver; copper oxide.**

INTRODUCTION

The low-temperature, complete oxidation of methane is an area in catalysis which, despite the large number of catalytic systems studied, does not yet have an adequate solution. The exhaust gas from natural gas-burning turbines and vehicles contains unconverted methane which is emitted into the atmosphere (currently unregulated). Methane is the most refractory of hydrocarbons, and its combustion requires temperatures higher than typical exhaust temperatures (400°C) (1). However, catalysts currently available (noble metals—Pd, Pt) are not adequate for low-temperature methane combustion, because they require a fairly high temperature for 100% conversion of methane (1).

The most active catalysts for methane oxidation are Pd-based catalysts and they have been extensively studied (2–6). However, the nature of active sites and sensitivity to Pd/PdO structure are not well understood (7,8). Pd-based catalysts are also strongly inhibited by the presence of reaction products (CO_2 and H_2O), as reported by Ribeiro *et al*. (4). In addition, they give partial oxidation products (CO and H_2) under reducing conditions (9). Other metal oxides studied include perovskite-like compounds (10–12), metal-exchanged zeolites (13–16), and transition metal oxides (17).

The methane oxidation rate on Pd-based catalysts is first order in methane, almost zero order in oxygen, and is strongly inhibited by reaction products (water and carbon dioxide) (4,7,8). Kinetic data are consistent with the Langmuir–Hinshelwood reaction mechanism, which includes dissociative adsorption of methane and oxygen. On the other hand, methane oxidation on metal oxides (perovskites) is usually treated using the redox mechanism (10,12). In both cases the abstraction of the first hydrogen atom is considered to be the rate limiting step.

In this work we approach methane activation through the surface active oxygen species of mixed metal oxides. We use cerium oxide as an active support for transition metals/metal oxides, such as silver and copper.

Cerium oxide is an excellent catalyst for redox reactions. The most important application is its use as an additive in the three-way catalyst (TWC) for automotive exhaust gas treatment. Use of ceria as an active support for methane and CO oxidation reactions was recently reported (18,19). Also, Cu-modified, doped cerium oxide materials were found to be excellent catalysts for the SO_2 reduction by CO (20,21). In general, the high activity of ceria in redox reactions has been attributed to the ceria reducibility and its high oxygen storage capacity (OSC) (22–25), and formation of defects, such as oxygen vacancies (26–28). Also, an advantage in the TWC context, is the ability of ceria to disperse transition metals and to increase the thermal stability of the alumina support (29,30).

The bulk and surface properties of CeO_2 can be modified by doping (30). Doping can improve the sintering properties of ceria, by stabilizing the ceria surface area and crystal size. Doping with divalent and trivalent dopants leads to formation of oxygen vacancies, and modification of oxygen mobility and ionic conductivity (28). The reduction properties and oxygen storage capacity of ceria are also reported

[1] Corresponding author.

0021-9517/98 $25.00

to change by doping. Ce-Zr-O solid solutions were extensively studied recently because of their unusual reduction behavior and high oxygen storage capacity (31). Zr and Hf doped CeO_2 were found to be good catalysts for methane combustion (32) and oxidation of isobutane (25). The reducibility and higher oxygen storage capacity of Ce-Zr-O solid solutions were attributed to the formation of defective fluorite structure by introduction of the smaller Zr^{4+} ion into the structure, which leads to higher oxygen mobility (24). In addition Balducci *et al.* (23) reported promotion of the redox behavior of Ce-Zr-O solid solutions upon sintering at high temperatures (1000°C).

Addition of noble metals (Pt, Pd, Rh) increases the reactivity of the low-temperature oxygen species formed on ceria (29, 33–39). As a result, the reducibility of ceria at low temperatures is enhanced (40,41). Recent reports have shown that the oxidation activity of ceria can be largely enhanced not only by the platinum metals but also by transition metals in general (42–44). However, the interaction of nanocrystalline ceria with metals and its ensuing higher activity in oxidation reactions is not well understood.

In the present paper we focus on the catalytic activity of nanocrystalline ceria and Cu and Ag-modified ceria for the complete oxidation of methane. La and Zr were used as dopants to modify the crystal size and sintering properties of ceria. The dependence of the catalyst on ceria reducibility, crystal size, and formation of extrinsic oxygen vacancies was examined. We report on the enhancement of the reduction properties and activity of ceria in redox reactions introduced by doping and by addition of transition metal/metal oxides (Ag and Cu). The interaction of ceria with Ag and CuO is a strong function of ceria crystal size. In the presence of a transition metal, a small crystal size of ceria favors the formation of highly reducible oxygen species.

EXPERIMENTAL

Catalyst Preparation

Doped fluorite-type oxides were synthesized by coprecipitating nitrate salts by urea at about 100°C (45). Approximately 25 mmol $(NH_4)_2Ce(NO_3)_6$ (Aldrich, 99.99%) and the desired amount of doping elements $ZrO(NO_3)_2$ (Aldrich, 99.99%), $La(NO_3)_3 \cdot 5H_2O$ (Aldrich, 99.9%), and 24 g of urea (99%, A.C.S. grade, Aldrich) were dissolved in 200 cm^3 deionized water. The solution was heated to 100°C and continuously mixed using a magnetic stirrer. After coprecipitation, the resulting gels of Ce and Zr were vigorously boiled for 8 h at 100°C to remove excess urea and age the gels. After aging, the precipitate was filtered, washed twice in boiling deionized water, and dried in a preheated vacuum oven (80–100°C) overnight. Only slight vacuum was applied (5 mmHg). Dried samples were crushed and calcined in air typically at 650°C for 8 h. The heating rate was 2°C/min. For comparison, CeO_2 was also made from cerium-acetate (Aldrich, 99.9%) decomposition at 750°C.

Copper modified fluorite-type oxides were prepared by the above urea coprecipitation–gelation method. Catalysts containing Ag were prepared by the incipient wetness impregnation method using the calcined supports prepared as above. The required amount of ammonia solution of $AgNO_3$ was added dropwise to the support powder under constant stirring. The wet powder was degased in vacuum for 1 h so that the solution fully filled the pores of the support. The samples were dried at 100°C overnight and calcined typically at 650°C for 8 h (heating rate 2°C/min).

The catalyst composition throughout the paper is expressed as atomic percentage (metal/total metals × 100%).

Catalyst Characterization and Testing Procedures

For bulk composition analysis the catalysts were analyzed by inductively coupled plasma (ICP) Atomic Emission Spectrometry (Perkin Elmer Plasma 40). The total BET surface area was routinely measured by single-point N_2 adsorption and desorption on a Micromeritics PulseChemiSorb 2705 instrument.

X-ray powder diffraction (XRD) analysis of catalyst samples was performed on a Rigaku 300 X-ray Diffractometer with Rotating Anode Generators and monochromatic detector. Copper K_α radiation was used with power setting at 60 kV and 300 mA. For crystal phase identification, the typical operation parameters were: divergence slit of 1°, scattering slit 1°, receiving slit 0.3°, and a scan rate 2–5°/min with 0.02° data interval.

The catalyst surface composition was determined by X-ray photoelectron spectroscopy (XPS) on a Perkin-Elmer 5100 system. For XPS analysis, the catalyst powder was pressed on a copper foil and placed in the vacuum chamber without any pretreatment. Mg X-ray source was used with the power setting at 300 W.

The catalyst microstructure analysis was performed on a Vacuum Generators HB603 scanning transmission electron microscope (STEM) equipped with X-ray microprobe of 0.14-nm optimum resolution for energy dispersive X-ray analysis (EDX). For STEM analysis, the catalyst powder was dispersed on a copper or nickel grid coated with a carbon film and elemental maps were obtained on a 128×128 data matrix. Ag/ZrO_2 catalysts were also analyzed by HRTEM/EDX. The analysis was performed on a JEOL 2010 instrument. The powder was suspended in isopropyl alcohol using an ultrasonic bath and deposited on the carbon-coated 200 mesh Cu grid.

All catalysts were tested in a laboratory-scale packed-bed flow reactor, which consisted of 1-cm ID × 50 cm long quartz tube with a porous quartz frit placed at the middle.

An electric furnace (Lindberg) was used to heat the reactor. Temperature was monitored by a K-type thermocouple placed at the top of the catalyst bed and controlled by a Wizard temperature controller. The flow of reacting gases was measured by mass flow meters. The typical feed gas was 1% CH_4, 8% O_2, balance He, for methane oxidation activity tests. All gases were certified calibration gas mixtures. The catalyst loading was 150 mg, unless otherwise noted. The typical catalyst packing density was 1.8 g/cm^3. The pressure drop through the reactor was <2 psi, so that all experiments were carried out at nearly atmospheric pressure. The catalysts were tested as prepared without any pretreatment (particle size <153 μm), and activity measurements were conducted in ascending temperature mode, so that light-off behavior could be recorded. In some experiments the activity was checked in descending manner to check for possible deactivation or hysteresis. A fixed contact time of 0.09 g · s/cm^3 (STP) (corresponding to a gas hourly space velocity, GHSV of 72,000 h^{-1}) was used in these experiments, unless otherwise noted. The product gas stream was analyzed by an HP 5880A gas chromatograph equipped with a 1/4 in. Carbosphere column (for CO, CO_2, and CH_4 separation) and a thermal conductivity detector. The carrier gas was helium at a flow rate of 30 cm^3/min (STP). The injector, oven, and detector temperatures were set at 90, 90, and 150°C, respectively. For kinetic measurements, the reactor was operated in the differential mode, with the conversion not exceeding 10%. The total flow rate was 200 cm^3/min (STP). The catalyst was diluted by a silicon carbide powder to achieve the short contact times (0.006–0.02 g · s/cm^3) needed for operation in the kinetically controlled regime. The particle size used in the kinetic experiments was <50 μm.

Temperature-programmed reduction (TPR) experiments by H_2 and CH_4 were performed in a thermogravimetric analyzer (TGA) with about 5-mg catalyst loaded in the pan (particle size <53 μm). Prior to reduction the catalyst was pretreated by heating to 650°C (10°C/min) for 30 min in 20% O_2/He at a flow rate of 500 cm^3/min (STP), followed by cooling (40°C/min) in the same gas mixture to room temperature. Flushing with He at room temperature was then used. The reduction gas was 5% H_2/He mixture at a flow rate 500 cm^3/min (STP). The heating rate was typically 10°C/min.

CH_4-TPR by methane was also performed in the laboratory-scale packed-bed reactor. Typically 200-mg catalyst was used for testing. Pretreatment included heating the catalyst in a flow of 10% O_2/He mixture (60 cm^3/min (STP)) to 650°C at a heating rate 10°C/min, followed by cooling to room temperature in 10% O_2/He mixture, and flushing with He at room temperature. A 5% CH_4/He gas mixture at a flow rate of 60 cm^3/min was used for reduction. The outlet gas was analyzed by a quadrupole mass spectrometer (MKS-model RS-1).

Oxygen uptake of Ag-containing catalysts was measured by a Micromeritics PulseChemiSorb 2705 instrument. Typically 0.1 g of catalyst was reduced at 170°C and 450°C in a flow of 10% H_2/He for 1 h and degased at 300°C and 470°C for 1.5 h, respectively. Oxygen uptake was then measured at 170°C by injecting pulses of 20% O_2/He. The oxygen uptake of the bare support was also measured for comparison.

RESULTS

Activity Tests

The properties of the materials used in this study are shown in Table 1. The doped cerias were characterized by BET surface area and crystal size determined from the ⟨111⟩ and ⟨220⟩ XRD peaks using the Scherrer equation, as shown in Table 1. The urea precipitation–gelation method leads to formation of nanocrystalline materials. All catalysts shown have the cubic crystal structure of fluorite-type oxides. Results indicate that doping stabilizes the ceria crystal size and its resistance to sintering (grain coarsening) in agreement with previous reports (46,47). Zr-doped catalysts calcined at 650°C have smaller crystal size (6.8 nm) than undoped CeO_2

TABLE 1

BET Surface Area and Crystal Size of Pure and Doped CeO_2

Catalyst (calcination temperature)	BET surface area (m^2/g)	Crystal size (nm) ⟨111⟩	Crystal size (nm) ⟨220⟩
CeO_2 (650°C)	70.2	9.4	9.1
CeO_2 (700°C)	37.8	13.5	13.0
CeO_2[a] (750°C)	18	20.0	—
CeO_2 (800°C)	0.3	24.4	21.6
Ce(10%Zr)O_2 (500°C)	138	5.3	4.9
Ce(10%Zr)O_2 (650°C)	101	6.8	6.3
Ce(10%Zr)O_2 (800°C)	38.9	10.1	10.5
Ce(50%Zr)O_2 (500°C)	119.9	4.1	4.0
Ce(50%Zr)O_2 (800°C)	32.2	7.8	6.4
Ce(4.5%La)O_2 (650°C)	69.1	8.1	8.5
Ce(10%La)O_2 (650°C)	91.7	7.2	7.7
Ce(10%La)O_2 (800°C)	41.9	12.5	12.9
5%Ag/ZrO_2 (650°C)	24.2		
3.5%Ag/ZrO_2 (650°C)	22.1		
2%Ag/ZrO_2 (650°C)	30.1		
5%Ag/CeO_2 (650°C)	12.4	23.2	22.9
3.4%Ag/CeO_2[a]	17.6	29.8	31.1
5%Ag/Ce(4.5%La)O_2 (650°C)	43.7	12.1	11.3
2%Ag/Ce(4.5%La)O_2 (650°C)	40.9	13.1	13.0
5%Ag/Ce(10%Zr)O_2 (650°C)	47.1	9.4	8.2
5%Ag/Ce(50%Zr)O_2 (650°C)	44.1	6.8	5.6
5%Cu/Ce(4.5%La)O_2 (650°C)	92.1	12.1	12.5
15%Cu/Ce(4.5%La)O_2(650°C)	32.3	n.d.	n.d.
5%Cu/Ce(50%Zr)O_2 (650°C)	87.6	n.d.	n.d.

[a] From acetate decomposition.

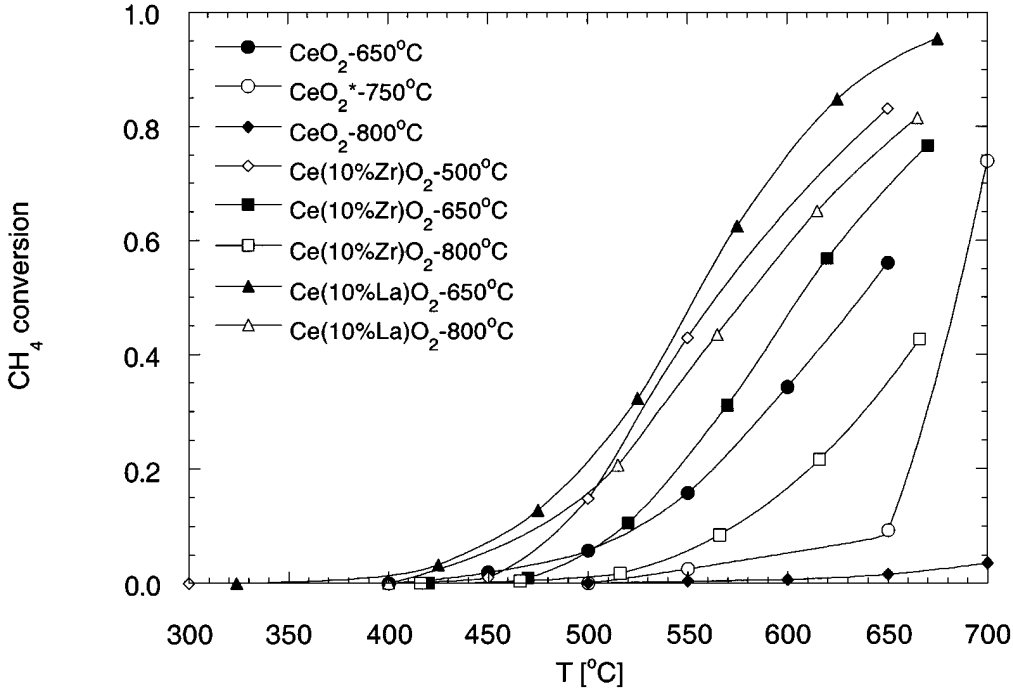

FIG. 1. Effect of heat treatment of doped CeO_2 (properties in Table 1) on methane oxidation; light-off performance; 0.09 g · s/cm^3 (STP), 1% CH_4, 8% O_2, balance He.

(9.4 nm). La-doped CeO_2 after the 650°C-calcination had intermediate crystal size (∼8 nm). When heated to 800°C in air, Zr-doped cerias grow in crystal size close to the La-doped ones.

Ce-Zr-O solid solutions with Zr content <50 at% exist in tetragonal and cubic form (48). In addition, metastable tetragonal phases are also formed (22, 49–52). The tetragonal crystal structure in Ce(50% Zr)O_2 could not be identified clearly due to the small particle size and, consequently, broad XRD peaks.

Cerium oxide is known to catalyze the complete oxidation of methane. When used as a support it is an active catalyst component. The performance of doped CeO_2 catalysts in methane-lean oxidation is shown in Fig. 1. At GHSV = 72,000 h^{-1}, the onset of methane oxidation (conversion ∼1%) is found for all doped CeO_2 at temperatures higher than 400°C, at the conditions of Fig. 1. Cerium oxide has a fluorite oxide-type crystal structure and oxygen vacancies as intrinsic defects. Introduction of La or Zr into ceria lattice decreases the crystal size of ceria and stabilizes its surface area. Zirconia as a tetravalent dopant does not introduce extrinsic oxygen vacancies in the ceria structure. On the other hand, La as a trivalent dopant, not only prevents the ceria crystal growth, but also creates extrinsic oxygen vacancies.

A strong effect of the CeO_2 crystal size and surface area on methane oxidation was observed. The CeO_2 prepared by urea precipitation (after 650°C calcination) gives higher CH_4 conversion at lower temperatures than the CeO_2 prepared by acetate decomposition (750°C). To examine this effect, selected catalysts were further calcined in air at 800°C for 8 h. In all cases, reduction of surface area and increase in the crystallite size of ceria resulted in reduced methane conversion at the conditions of Fig. 1. Undoped ceria lost its activity completely after the 800°C treatment. La-doped CeO_2 retained high methane oxidation activity despite a reduction of surface area (crystal size growth) after high temperature treatment (800°C, 8 h), as shown in Fig. 1. Zr-doped ceria, however, lost much of its activity after the 800°C-treatment. The activity change as a result of the 800°C treatment can not be solely attributed to the reduction of surface area and to crystal growth of ceria. La-doped ceria has approximately the same surface area as Zr-doped ceria (∼40 m^2/g) after the 800°C calcination, but the activity of the former is higher. Data in Fig. 1 illustrate the complex relation between the ceria properties and its performance in methane oxidation. The latter also depends on the presence of surface defects (oxygen vacancies), which can be formed by introduction of a trivalent dopant (La) into the ceria structure. Surface defects are also created by decreasing the crystal size of ceria.

La- and Zr-doped cerium oxide were chosen for kinetic studies. Variation of the CH_4 oxidation rate over the Ce(10% La)O_2 catalyst with the partial pressure of methane (P_m) and partial pressure of oxygen (P_o) is shown in Figs. 2 and 3, respectively. The methane oxidation rate increased as P_m increased at constant P_o. At constant P_m, the reaction rate increased slowly as P_o was increased. Methane

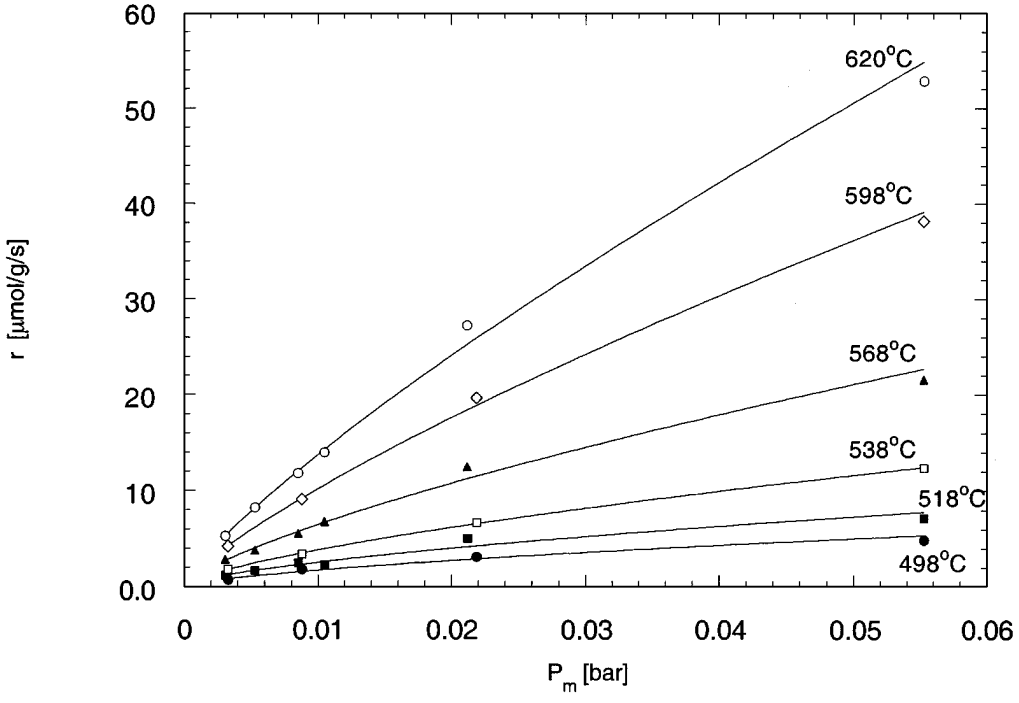

FIG. 2. Variation of methane oxidation rate with partial pressure of methane, under constant oxygen pressure, $P_o = 0.05$ bar; Ce(10%La)O_2 calcined at 650°C (Table 1).

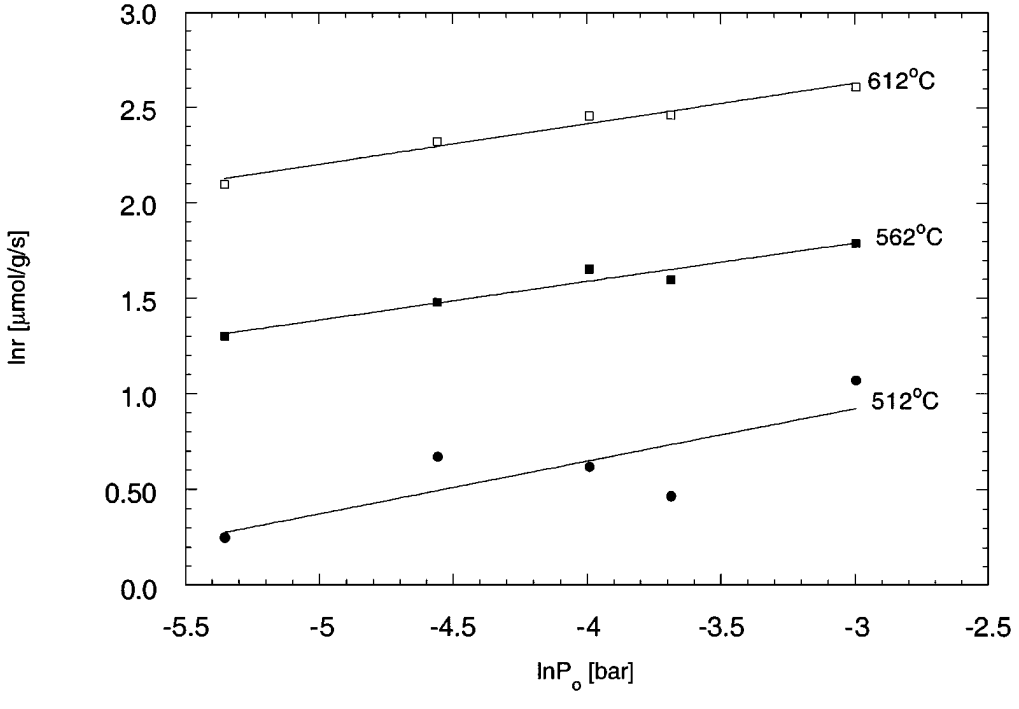

FIG. 3. Variation of methane oxidation rate with partial pressure of oxygen under constant methane pressure $P_m = 0.01$ bar; Ce(10%La)O_2 calcined at 650°C (Table 1).

TABLE 2

Methane Oxidation Kinetics over Ce(10% La)O_2 and 15% CuCe(4.5% La)O_2 Catalysts[a]

	Equation (4)		Equation (1)			
	A' [μmol/g/s/bar$^{1.23}$]	Ea' [kJ/mol]	A[b] [μmol/g/s/bar$^{0.23}$]	Ea [kJ/mol]	K [1/bar]	Q [kJ/mol]
Ce(10% La)O_2	$8.9 \cdot 10^9$	113.0	$5.7 \cdot 10^8$	113.0	1.03	24.3
15% CuCe(4.5% La)O_2	$5.9 \cdot 10^{10}$ [c]	119.3[c]	$7.84 \cdot 10^7$ [d]	93.4[d]	3.46[d]	14.2[d]

[a] Calcined at 650°C (Table 1).
[b] For 15% CuCe(4.5% La)O_2 in μmol/g/s/bar$^{0.18}$.
[c] This work, BET surface area = 32.3 m^2/g.
[d] From Liu and Flytzani-Stephanopoulos (1995) (18,19), BET surface area = 30 m^2/g.

oxidation on noble metal catalysts is usually interpreted based on the Langmuir–Hinshelwood mechanism which includes dissociative adsorption of methane and oxygen (7,8), with the abstraction of the first hydrogen atom being the rate limiting step. On the other hand, methane oxidation on metal oxides is usually treated using the redox mechanism (10–12). The experimental data (Figs. 2 and 3) were best represented by

$$r = k_m K_m P_m P_o^{0.23} / (1 + K_m P_m), \quad [1]$$

where k_m is the surface reaction rate,

$$k_m = A \exp(-E_a/RT), \quad [2]$$

and K_m, the CH_4 adsorption equilibrium constant,

$$K_m = K \exp(Q/RT). \quad [3]$$

The Langmuir adsorption-type dependence on P_m in Eq. (1) suggests that the rate-determining step involves adsorbed methane. The power order dependence on the partial pressure of oxygen suggests a complex oxygen source for the reaction. Due to the low value of the heat of adsorption, Q (24.3 kJ/mol, Table 2), the experimental data may be represented by a simpler kinetic expression,

$$r = k'_m P_m P_o^{0.23}, \quad [4]$$

$$k'_m = A' \exp(-Ea'/RT), \quad [5]$$

The values of the kinetic parameters for methane oxidation over Ce(10% La)O_2 are listed in Table 2. The value of the heat of adsorption is low, 24.3 kJ/mol, and the activation energy is 113.0 kJ/mol.

Equation (4) is consistent with the redox mechanism of methane oxidation with a slow reduction and fast oxidation steps. Whether or not methane activation involves adsorbed methane species could not be determined by the methods used in this study.

Since both Eqs. (1) and (4) give satisfactory representation of the experimental data, we chose Eq. (4) to compare the various doped CeO_2 catalysts, subjected to different thermal treatment. Experiments were conducted under $P_m = 0.01$ bar and $P_o = 0.05$ bar, with conversion not exceeding 10%. Figure 4 shows Arrhenius plots for La- and Zr-doped CeO_2 and undoped CeO_2 for comparison. Reaction rates are normalized by the total BET surface area in order to compare specific activities. Measured reaction rates are in agreement with those reported for Ce(20% Zr)O_2 catalysts (32). The values of the kinetic parameters are shown in Table 3.

For undoped CeO_2, heating to high temperature (700°C) prior to reaction leads to a decrease in the preexponential factor, while the activation energy remains approximately the same (from 100.8 kJ/mol to 94.7 kJ/mol), indicating loss of active sites after the 700°C calcination in air, as the crystal size of ceria increases from 9.4 nm to 13.5 nm (Table 1). La-doped CeO_2 has the highest preexponential factor and activation energy (113.0 kJ/mol) among the catalysts studied. Calcination in air at 800°C does not significantly affect the kinetics of methane oxidation over Ce(10% La)O_2, despite the loss of BET surface area (from 91.7 to 41.9 m^2/g; Table 1). The surface area-normalized specific activity, however, increases as the crystal size is increased from 7.2 nm to 12.5 nm). Results indicate that the nature of active sites is changed after the high temperature treatment, which may

TABLE 3

Kinetic Parameters for Methane Oxidation over Various Doped CeO_2 Materials[a]

	A′ [μmol/m^2/s/bar$^{1.23}$]	Ea′ [kJ/mol]	Surface composition (at% dopant)[b]
CeO_2-650°C	9.6×10^6	100.8	—
CeO_2-700°C	2.9×10^6	94.7	—
Ce(10% Zr)O_2-650°C	1.4×10^6	85.7	7.1
Ce(10% Zr)O_2-800°C	10.8×10^6	107.2	5.8
Ce(10% La)O_2-650°C	9.6×10^7	113.0	12.1
Ce(10% La)O_2-800°C	28.4×10^7	116.2	13.8

[a] For the kinetic expression shown by Eq. [4]; see text.
[b] Determined by XPS.

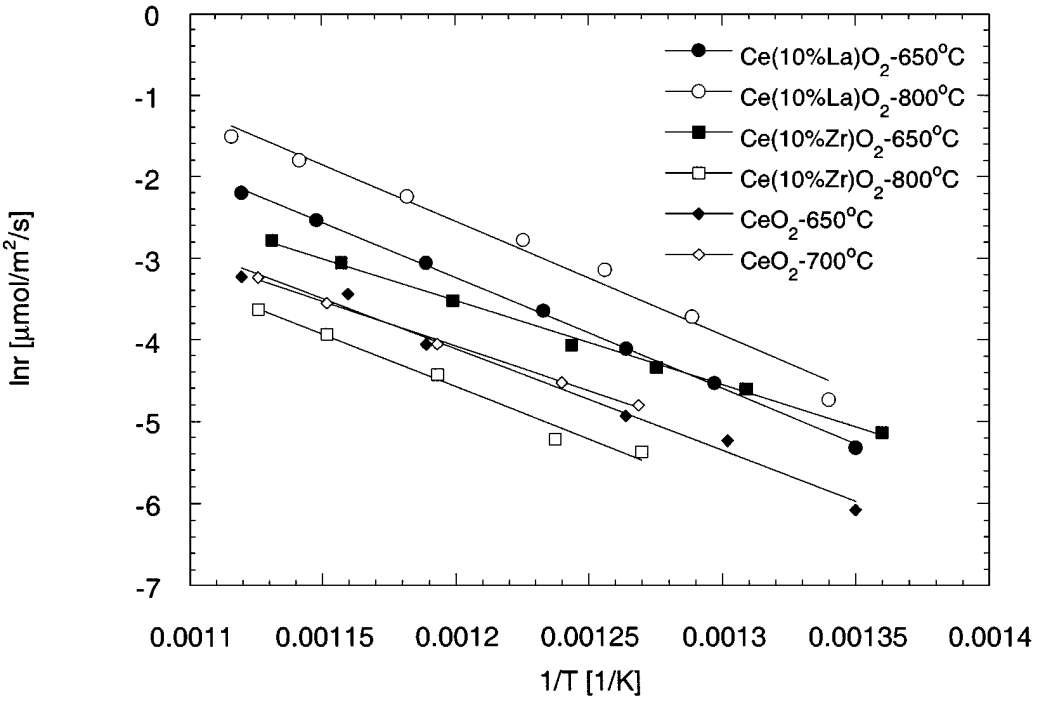

FIG. 4. Arrhenius-type plots for methane oxidation over undoped and doped CeO_2 catalysts; 0.04 g · s/cm^3 (STP), 1% CH_4, 5% O_2, balance He.

be attributed to La segregation to the surface (increase of La concentration from 12.1 to 13.8% as determined by XPS analysis). La enrichment of the surface of ceria was previously reported by Pijolat *et al.* (46). For Zr-doped CeO_2, the observed activation energy is lower that the activation energy for the undoped and La-doped CeO_2. This is probably related to the reducibility of Zr-doped CeO_2 and its small crystal size, 6.8 nm, as determined by XRD. After the 800°C calcination in air, the crystal size and kinetic parameters of the Zr-doped ceria approach those of undoped ceria (calcined at 650°C). The surface concentration of zirconia decreases after the 800°C calcination (Table 3). However, loss of the specific activity cannot be solely attributed to the surface composition change. It seems that some other structural changes, which could not be observed by the techniques used in this study occur at high temperatures.

The methane oxidation activity of ceria supported CuOx catalysts is shown in Fig. 5. Ceria-supported CuO_x catalysts have higher activity than the respective support, when compared on a rate per gram or per surface area basis. In this catalyst formulation copper is present in oxidized form (18,19,44). Copper oxide itself is an active oxidation catalyst. In a previous study we have reported on the effect of copper oxide dispersion and oxidation state on methane oxidation activity (53). In Cu-modified doped CeO_2 catalysts, copper exists as partially oxidized clusters, strongly associated with ceria (18,19). At high copper content (≥15 at%), in addition to copper clusters, dispersed CuO particles were identified by XRD and STEM/EDX. The activity of small (few nanometers) partially oxidized copper clusters is lower than that of dispersed copper oxide particles (∼10 nm) (53), when copper is supported on inert zirconia. Comparison of kinetic data for La-doped CeO_2 and Cu-modified La-doped CeO_2 showed that a similar kinetic expression may be used to represent the kinetics of methane oxidation on both catalysts (Table 2). The reaction order with respect to methane partial pressure is very close to 1, while the reaction order with respect to oxygen partial pressure is close to zero (0.23 for the La-doped and 0.18 for the Cu-modified material). When Eq. [1] is used to represent the kinetic data, the heat of adsorption of methane is low on both catalysts (24.3 kJ/mol for the La-doped material and 14.2 for the Cu-modified catalyst (44)), while the activation energy is significantly lower on Cu-modified catalysts, indicating that addition of Cu lowers the methane activation barrier. Comparison of reaction rates for Ce(10% La)O_2 (Table 2) and rates reported by Liu and Flytzani-Stephanopoulos (19) for 15% CuCe(4.5% La)O_2, shows that addition of Cu to La-doped CeO_2 increases the methane oxidation rates at low temperature (<500°C), while at temperature >500°C reaction rates approach those of La-doped CeO_2.

Although the structure of Ag catalysts is different, behavior similar to that of copper catalysts for methane oxidation is observed. XRD analysis of fresh, 650°C-calcined samples identified the presence of silver metal at low Ag concentrations (<10 at%), as shown in Fig. 6. Despite the loss of initial surface area of the support and ceria crystal

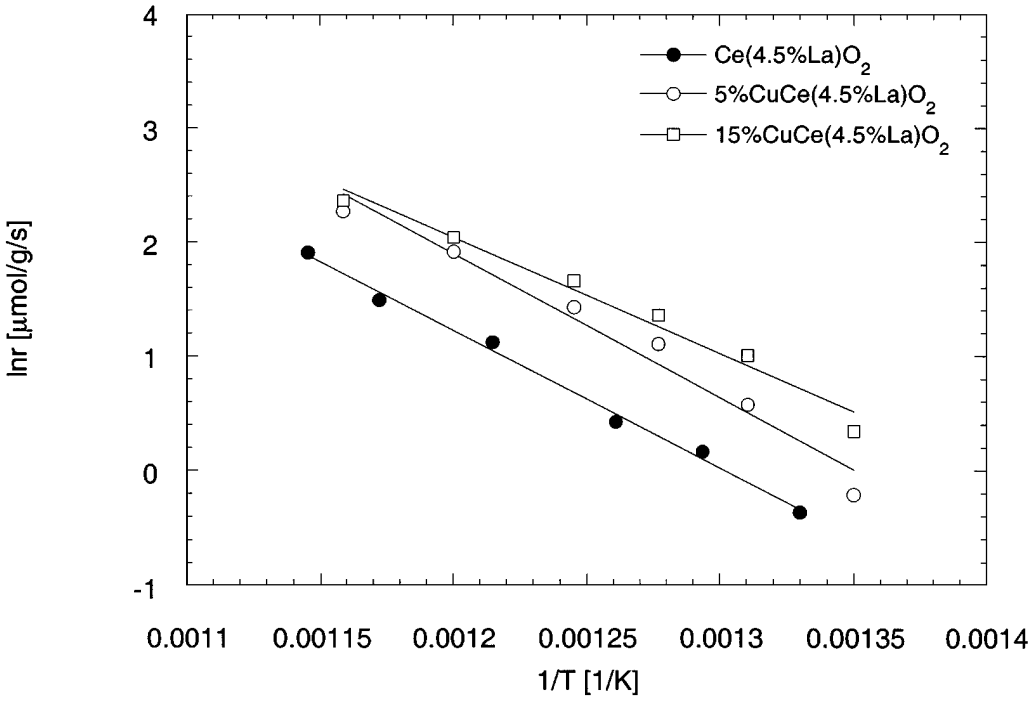

FIG. 5. Arrhenius-type plots for methane oxidation of Ce(4.5% La)O_2-supported copper catalysts; all catalysts calcined at 650°C (Table 1); 0.006–0.02 g · s/cm^3 (STP), 1% CH_4, 5% O_2, balance He.

growth (e.g., from ∼8 nm to ∼12 nm for the Ce(4.5% La)O_2 support) as a result of impregnation and calcination, Ag-modified catalysts have higher methane oxidation activity than the Ce(4.5% La)O_2 support, as shown in Fig. 7. The crystal size of the ceria support appears to play an important role. As the crystal size of ceria support decreases (from 12.1 nm for Ag/Ce(4.5% La)O_2 and 9.4 nm for Ag/Ce(10% Zr)O_2 to 6.8 nm for Ag/Ce(50% Zr)O_2), the activity

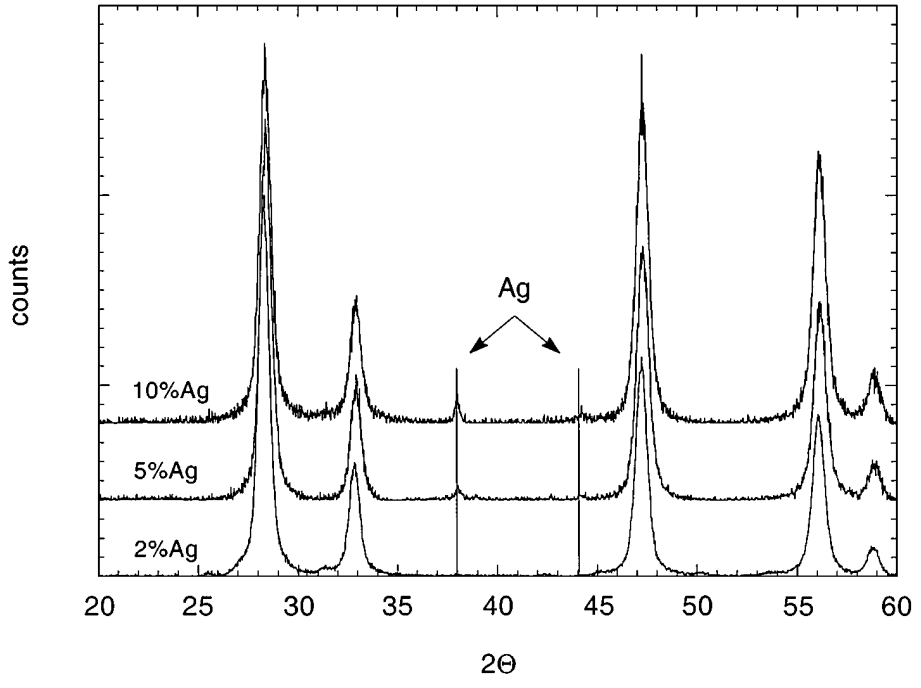

FIG. 6. XRD profile of Ag/Ce(4.5% La)O_2 catalyst; fresh—after 650°C calcination.

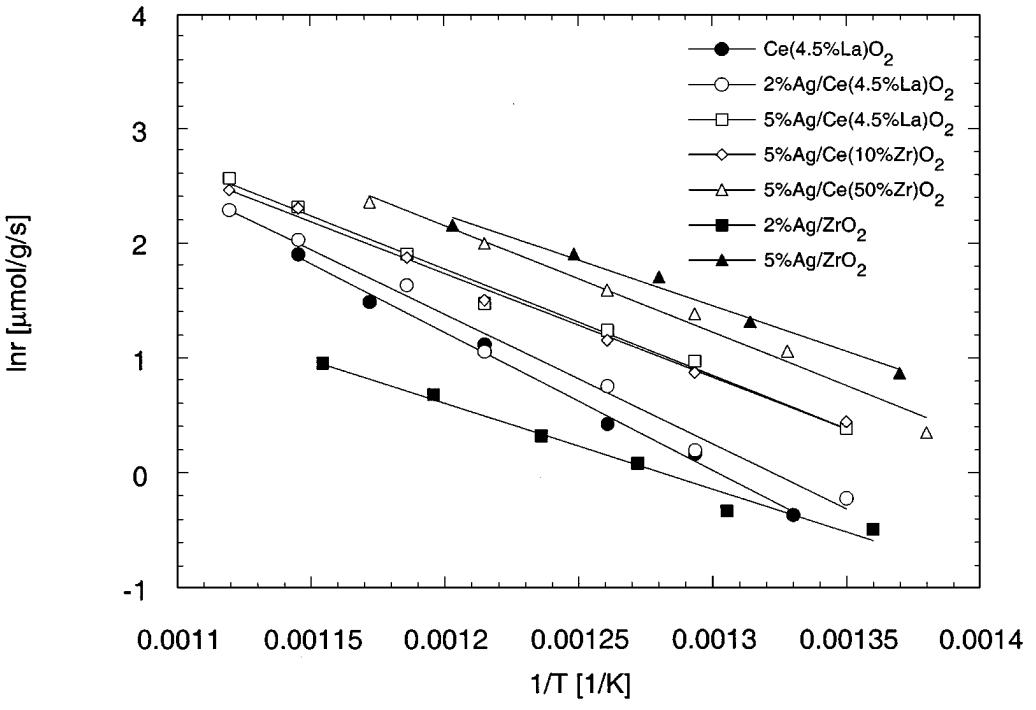

FIG. 7. Arrhenius-type plots for methane oxidation of CeO_2- and ZrO_2-supported Ag catalysts; all catalysts calcined at 650°C (Table 1); 0.006–0.02 g · s/cm^3 (STP), 1% CH_4, 5% O_2, balance He.

increases. Also increasing Ag loading from 2 to 5% increases the activity, as is shown for Ag/Ce(4.5% La)O_2. To separate the effect of the metal from that of the support, we also prepared silver supported on ZrO_2. At low metal loading (2%), the activity of the ceria-supported Ag is higher than that of zirconia-supported Ag. However, as shown in Fig. 7, the 5% Ag supported on ZrO_2 has activity similar to that of Ag supported on doped CeO_2 catalysts, although ZrO_2 itself did not have any activity for methane oxidation in the temperature range studied. Our recent data (54, 55) indicate that the structure of Ag particles has a strong effect on methane oxidation activity, with Ag supported on an inert support, such as zirconia or alumina. The turnover number for methane oxidation increases an order of magnitude as the Ag particle size increases from 5–10 nm (determined by HRTEM) (54,55).

Reduction Properties

Different oxygen species present in the doped CeO_2 catalysts were characterized using temperature programmed reduction by H_2. The reducibility of ceria has been extensively studied in the literature using temperature programmed reduction techniques (TPR). In reduction of ceria by H_2, a low-temperature peak (500°C) is attributed to the reduction of surface capping oxygen species, while a high-temperature reduction peak (800°C) is attributed to bulk reduction (29,40). More detailed studies of surface reduction of CeO_2 were reported (56–62).

Figure 8 shows plots of the weight change and the derivative of the weight change of each sample with temperature. Table 4 lists the TPR results in the form of reduction extent, x, of CeO_x. Surface reduction of undoped CeO_2 (Fig. 8a) starts around 300°C (Table 4, $x = 1.99$). Bulk reduction of

TABLE 4

Reduction Extent of Modified-Ceria Catalysts in H_2-TPR[a]

Catalyst (calcination temperature)	Reduction temperature (°C)							
	170	200	300	400	450	500	600	850
CeO_2 (650°C)	2.00	2.00	1.99	1.98	1.97	1.96	1.93	1.75
Ce(10%Zr)O_2 (500°C)	1.96	1.95	1.93	1.91	1.89	1.86	1.76	1.61
Ce(10%Zr)O_2 (650°C)	1.96	1.95	1.92	1.90	1.88	1.85	1.73	1.60
Ce(10%Zr)O_2 (800°C)	1.97	1.96	1.95	1.94	1.92	1.88	1.77	1.66
Ce(50%Zr)O_2 (500°C)	1.97	1.95	1.91	1.86	1.81	1.72	1.53	1.38[c]
Ce(50%Zr)O_2 (800°C)	1.99	1.99	1.98	1.95	1.92	1.87	1.68	1.50
Ce(4.5%La)O_2 (650°C)	2.00	2.00	1.99	1.98	1.98	1.96	1.90	1.75
Ce(10%La)O_2 (650°C)	1.97	1.96	1.96	1.94	1.93	1.91	1.84	1.73
Ce(10%La)O_2 (800°C)	1.99	1.99	1.98	1.97	1.97	1.95	1.89	1.75
5%CuCe(50%Zr)O_2 (650°C)[b]	1.87	1.84	1.76	1.69	1.64	1.59	1.52	1.38[c]
5%CuCe(4.5%La)O_2 (650°C)[b]	1.96	1.93	1.91	1.88	1.86	1.84	1.78	1.66

[a] Reduction extent expressed as x in CeO_x. TPR conditions: 5% H_2/He, 500 cm^3/min (STP), 10°C/min in a TGA.

[b] Reduction extent expressed as x in CeO_x, assuming that all CuO was reduced to metal.

[c] Values exceeding the Ce_2O_3 stoichiometry (see text).

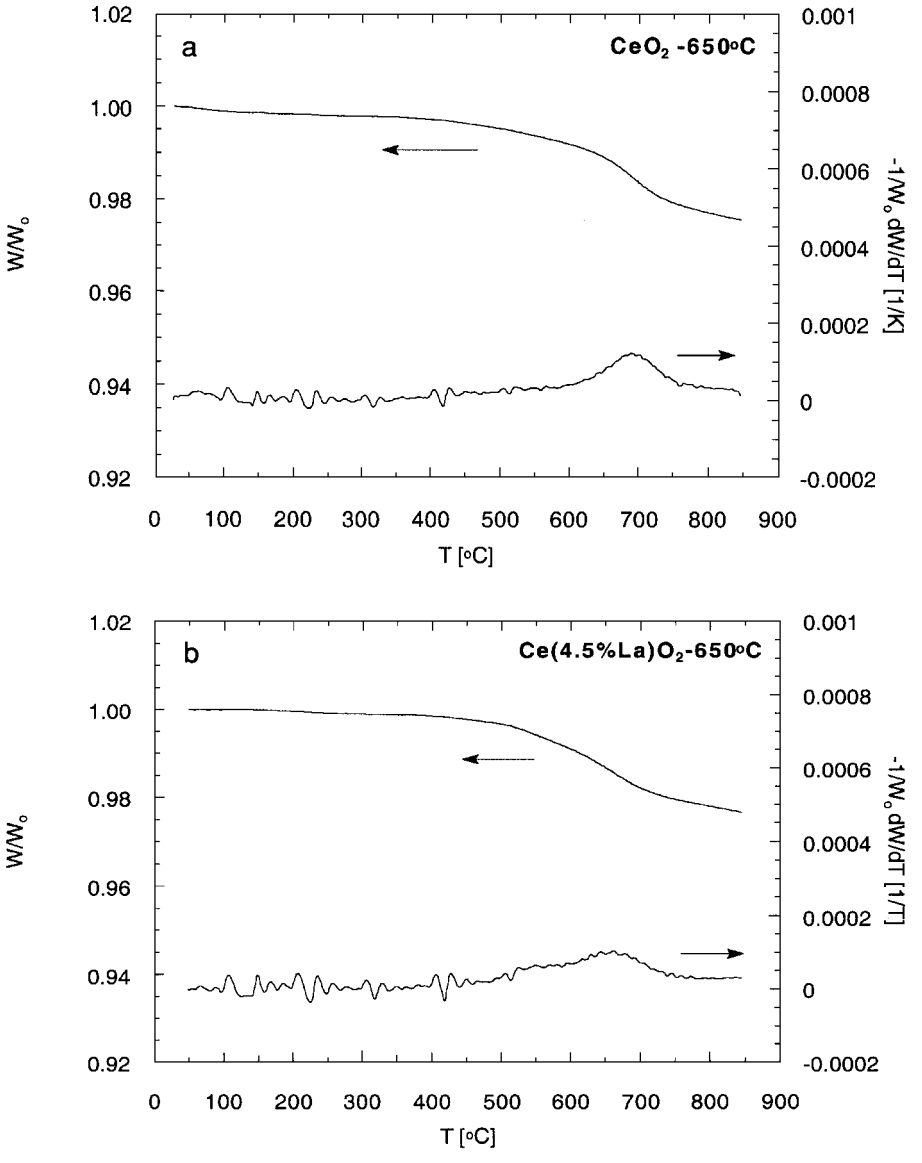

FIG. 8. H_2-TPR profiles of undoped and doped CeO_2; all after 650°C calcination (Table 1); 5% H_2/He, 500 cm^3/min (STP), 10°C/min: (a) CeO_2; (b) Ce(4.5%La)O_2; (c) Ce(10%La)O_2; (d) Ce(10%Zr)O_2.

CeO_2 occurs at higher temperatures with maximum rate at about 700°C (Fig. 8a). Doping with La changes the bulk reduction properties of ceria as shown in Fig. 8b for Ce(4.5% La)O_2 (at 600°C, $x = 1.90$ for Ce(4.5% La)O_2 compared to 1.93 for undoped ceria). The maximum reduction rate occurs around 650°C. The amount of surface oxygen reduced increases as the La level increases to 10 at%, and bulk reduction begins at lower temperature with maximum rate at 600°C (Table 4 and Fig. 8c). Similarly, the Zr-doped catalyst has lower reduction temperature than undoped CeO_2 as shown in Fig. 8d. Higher reducibility of Ce-Zr-O mixed oxides was recently reported by Fornasiero *et al.* (31). This was attributed to the higher oxygen mobility (oxygen conductivity) of Ce-Zr-O mixed oxides, due to structural changes introduced by doping. Here we find that the final reduction extent (at 850°C) for the Ce(50%Zr)O_2-containing materials exceeds the Ce_2O_3 stoichiometry (Table 4). The reasons for this behavior are not clear.

The effect of calcination temperature on the reducibility of Zr- and La-doped catalysts is shown in Table 4. Loss of surface area and crystal growth result in loss of surface oxygen for both types of materials. However, the bulk reduction properties are only slightly influenced by crystal growth. Bulk reduction of Ce(10% Zr)O_2 occurs at lower temperature than the Ce(10% La)O_2 catalyst even after high temperature annealing (Table 4).

The higher reducibility of doped ceria materials compared to undoped ceria was confirmed in CH_4-TPR. All

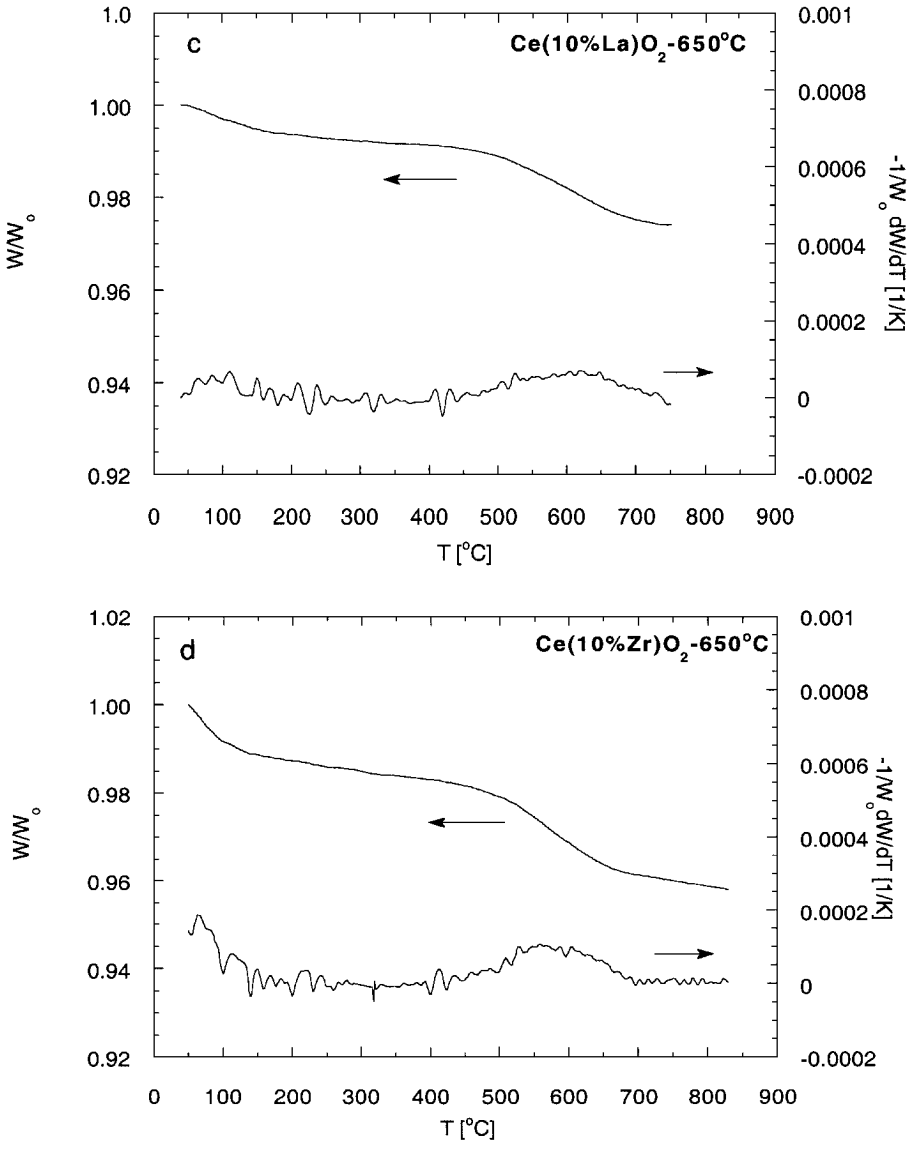

FIG. 8—*Continued*

CeO_2-based catalyst react with methane at temperatures higher than 400°C, which is the temperature range where steady-state activity was observed (Fig. 1). CO_2 and H_2O were the only reduction products below 650°C. At temperatures higher than 650°C H_2 and CO were detected, indicating the ability of partially reduced ceria to partially oxidize methane. Under the reaction conditions in this study, no partial oxidation products were observed. Figure 9 shows CO_2 evolution as a function of temperature for undoped and La- and Zr-doped ceria. As expected, reduction temperatures are higher (~400°C) than in H_2-TPR (~200°C) when methane is used as the reductant. The onset for the reduction in methane is the same for all catalysts studied (~400°C). Bulk and surface reduction of ceria occur simultaneously, probably because of the oxygen diffusion from the bulk to the surface at these high reduction temperatures. Higher slopes in the carbon dioxide evolution profiles indicate higher reduction rate for both La- and Zr-doped ceria than for undoped ceria.

It is well known that the presence of noble metals (Pt, Rh) can improve the ceria reducibility at low temperatures (26,29,40). Here we show that other transition metals induce similar behavior. Figure 10 shows H_2-TPR profiles of Cu-Ce(La)O_x and Cu-Ce(Zr)O_x catalysts. A low temperature peak which corresponds to CuO reduction is observed at 160°C for both supports. Literature data (63) show that the reduction peak of bulk CuO typically occurs between 200 and 300°C. The reduction temperature observed here is significantly lower than the bulk CuO reduction temperature, indicating that the CuO reducibility is enhanced by the presence of ceria. The bulk reduction of doped CeO_2 is not affected by the addition of copper. However, the reduction

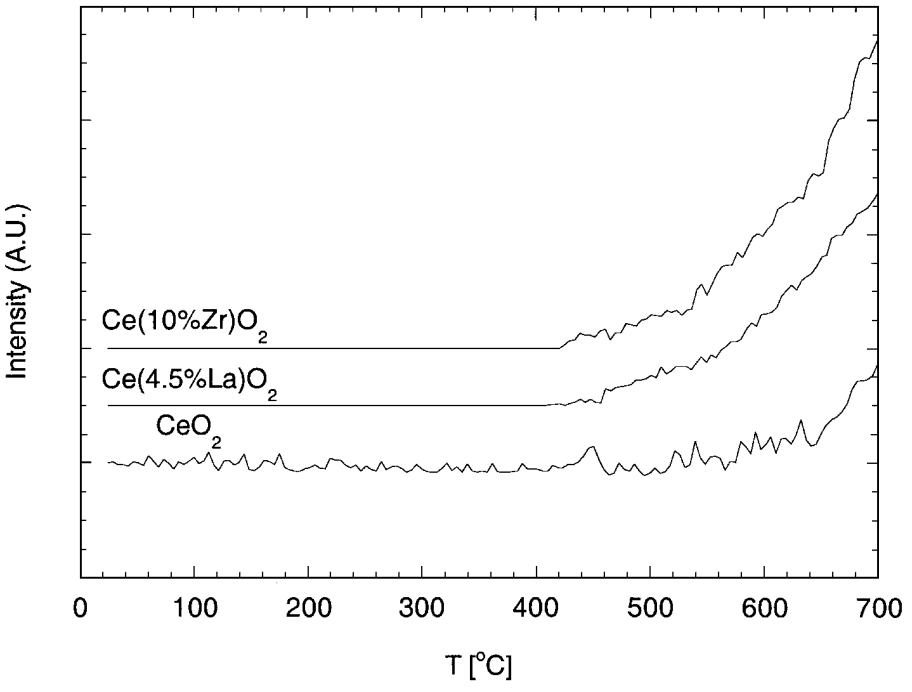

FIG. 9. CH_4-TPR profiles of undoped and doped CeO_2; all after 650°C calcination (Table 1); 5% CH_4/He, 60 cm^3/min (STP), 10°C/min.

extent shows that the surface oxygen reduction of Ce(4.5% La)O_2 is increased by the addition of copper (Table 4). The same effect of the addition of Cu was observed on Ce(50% Zr)O_2 (Table 4). This is in agreement with the previously reported enhancement of CeO_2 reducibility in physically mixed powders of nano-CuO and CeO_2 (64).

Figure 11 shows CH_4-TPR profiles of copper-modified catalysts in the form of CO_2 measured by mass spectrometry. These TPR tests were performed in the packed-bed reactor. Reaction of methane with these oxidized catalysts gives CO_2 and H_2O as the main reduction products. Only trace amounts of CO were observed at temperatures lower than 650°C. The onset of the reduction of a 5% CuCe(La)O_2 catalyst in CH_4-TPR is about 400°C, with maximum reduction rate at about 450°C. On the other hand, at a higher copper content (>5 at%), reduction starts at 300°C, and a doublet is observed. Reduction of bulk CuO (prepared by carbonate decomposition) is shown for comparison, indicating that the doublet in the reduction profile comes from bulk CuO reduction. At low copper content (5 at%) the amount of oxygen reduced exceeds the amount necessary for complete reduction of CuO to metallic copper (53). As in H_2-TPR, this is due to the enhancement of ceria reduction at low temperatures.

Ag-modified ceria showed different behavior. No distinct silver oxide reduction peaks were observed in H_2-TPR, which is in agreement with our XRD data which showed the presence of metallic silver. The absence of a surface reduction peak is attributed to the low surface area of the Ag-modified samples. Although active oxygen important in methane oxidation could not be identified by the H_2-TPR experiments of Ag-doped cerias, oxygen uptake experiments after reduction at 170°C and 450°C indicates availability of oxygen for oxidation reactions on these catalysts. This is strongly influenced by the nature of the support. Table 5 summarizes the oxygen uptake of various Ag-modified doped CeO_2 catalysts. Oxygen uptake of the bare supports was also measured for comparison. This is expressed as reduction extent x in CeO_x. Under the conditions of the uptake experiments, both ceria and Ag adsorb oxygen. Their separate contributions could not be calculated exactly. The reduction extent of ceria in Ag modified materials was calculated after the total oxygen uptake was corrected for oxygen adsorbed on Ag (assuming all Ag was oxidized to Ag_2O, according to the preferred stoichiometry at 170°C (65)). A Ag : O stoichiometry needs to be used to calculate the extent of ceria reduction. Thus, the reduction extent of ceria is a lower limit, since all Ag was assumed to be fully exposed (100% dispersed). Ag was found in the metallic state after the oxygen uptake experiments, as it is in the fresh catalyst (determined by XRD).

Neither the undoped nor the La- and Zr-doped CeO_2 catalysts had measurable oxygen uptake after reduction at 170°C. After reduction at 450°C, the oxygen uptake of undoped and La-doped CeO_2 was the same, while Zr-doped CeO_2 had the highest uptake. The oxygen uptake of Ag-modified catalysts, however, clearly showed a synergism between the metal and the support. Indeed, the oxygen uptake after the 170°C-reduction was much higher than would correspond to Ag alone, even if all Ag was oxidized with

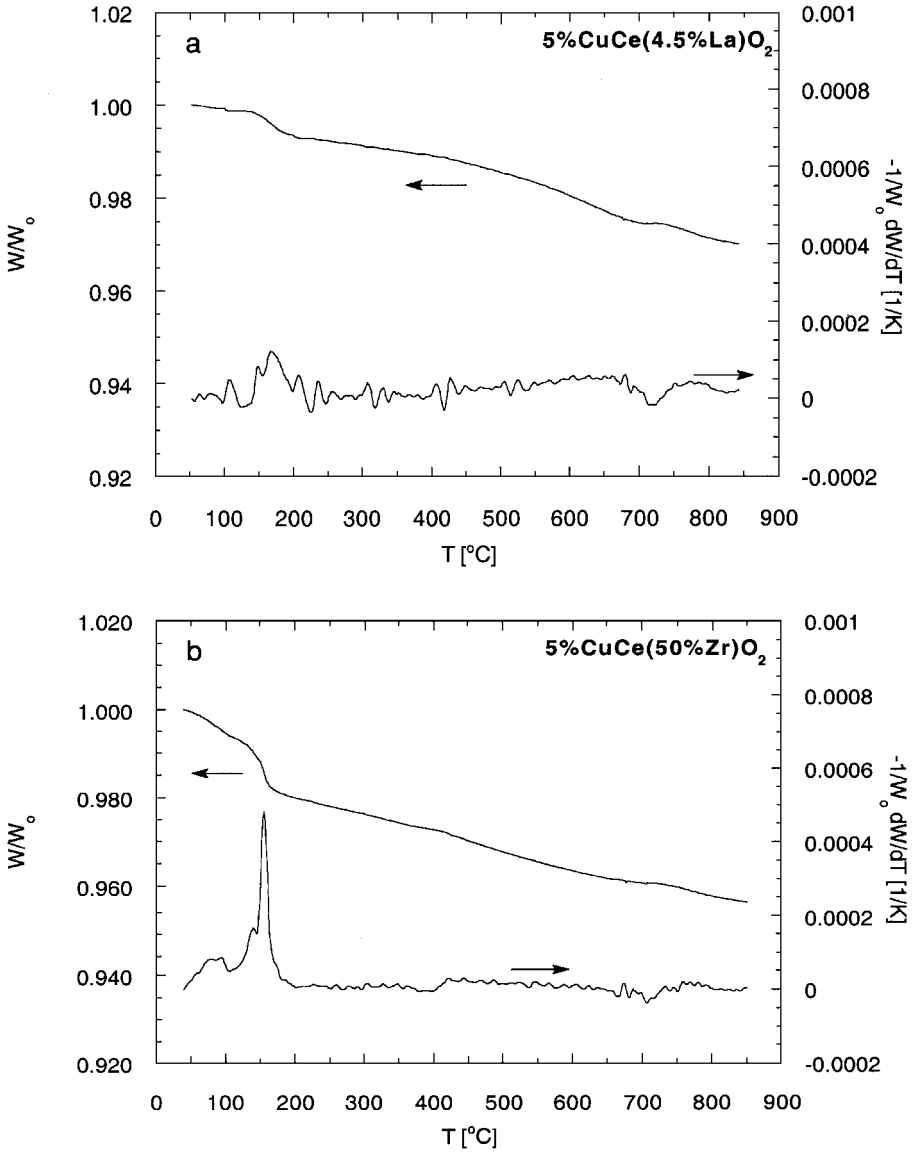

FIG. 10. H_2-TPR profiles of Cu modified doped CeO_2 catalysts; fresh—after 650°C calcination (Table 1); 5% H_2/He, 500 cm^3/min (STP), 10°C/min.

one-to-one stoichiometry. The excess oxygen must have been adsorbed on surface oxygen vacancies formed on the support. After reduction at 450°C, however, the reduction extent of the Ag-modified CeO_2 was similar to the reduction extent of the bare support at the same conditions.

The crystal size of ceria has a major influence on the measured oxygen uptake. CeO_2 (24.2 nm) and Ce(4.5% La)O_2 (12.1 nm) supported Ag catalysts have lower oxygen uptake than the Ag/Ce(x% Zr)O_2 (9.4 nm for 10% Zr and 6.8 nm for 50% Zr) catalysts after reduction at 170°C. The calculated dispersion (64.2% for 5% Ag/CeO_2 and 85.4% for 5% Ag/Ce(4.5% La)O_2) is, however, high for this Ag loading, especially if compared to the 5% Ag/ZrO_2 catalyst (9.5%, Table 5), so that participation of the support is clearly indicated.

DISCUSSION

Kinetic expressions for the methane oxidation reported in the literature for both noble metals and metal oxides are first order in methane partial pressure and almost zero order in oxygen partial pressure. Kinetic data for Pd-based catalysts are consistent with the reaction steps based on the Langmuir–Hinshelwood mechanism which includes dissociative adsorption of methane and oxygen (4,7,8). The abstraction of the first hydrogen atom from methane is considered to be the rate-limiting step. On the other hand, methane oxidation on metal oxides (perovskites) is usually treated using the Mars–van Krevelen redox mechanism (10,13). In the case of slow surface reduction by methane and fast reoxidation by oxygen, first order in methane

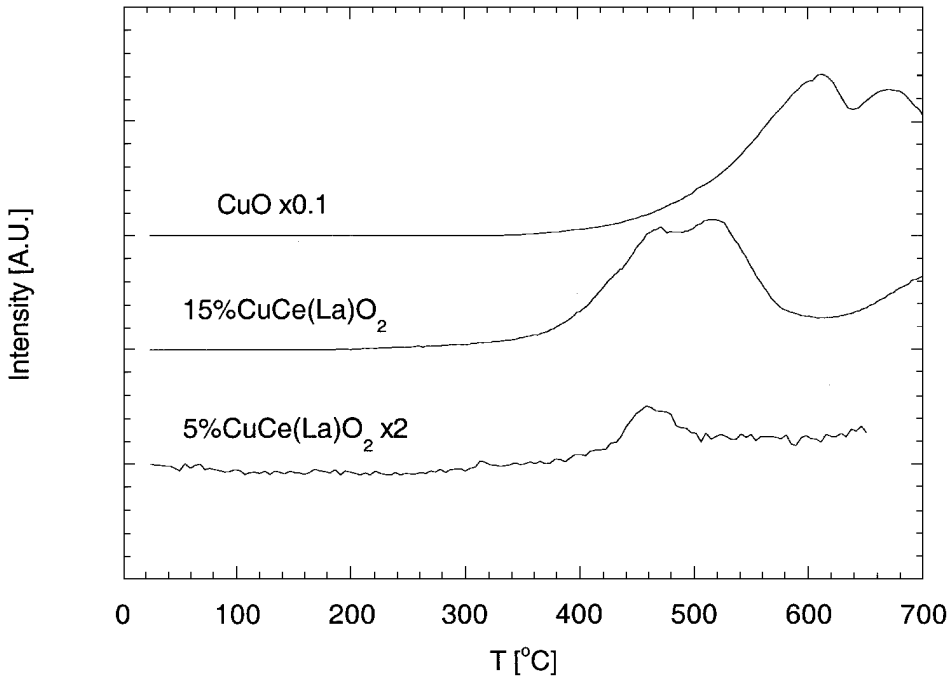

FIG. 11. CH_4-TPR profiles of Cu modified doped CeO_2 catalysts; fresh—after 650°C calcination (Table 1); 5% CH_4/He, 60 cm^3/min (STP), 10°C/min.

partial pressure, and zero order in oxygen partial pressure are obtained.

The kinetic data reported here for methane oxidation on doped ceria are in agreement with those reported in the literature for similar systems. We demonstrated using CH_4-TPR that doped ceria materials can be reduced by methane, so that the redox mechanism cannot be excluded. Ceria surface can be reduced by methane at temperatures higher

TABLE 5

Oxygen Uptake of Ag Modified Doped CeO_2 Catalysts[a]

Catalyst	Reduction temperature (°C)	x in CeO_x[d]	Catalyst	Reduction temperature (°C)	x in CeO_x[d]	Dispersion[c] [%]	mol O_2/mol Ag[b]
			3.5% Ag/CeO_2*[e]	170	2.00	24.4	0.061
CeO_2	170	2.00	5% Ag/CeO_2	170	2.00	64.2	0.16
	450	1.99		450	1.98		0.84
Ce(10% Zr)O_2	170	2.00	5% Ag/Ce(10% Zr)O_2	170	1.99		0.443
	450	1.98		450	1.98		0.898
Ce(50%Zr)O_2	170	2.00	5% Ag/Ce(50% Zr)O_2	170	1.98		0.729
	450	1.95		450	1.95		1.145
Ce(4.5%La)O_2	170	2.00	5% Ag/Ce(4.5% La)O_2	170	2.00	85.4	0.213
			2% Ag/Ce(4.5% La)O_2	170	2.00	99.0	0.247
			5% Ag/ZrO_2	170		9.53	0.024
			3.5% Ag/ZrO_2	170		25.6	0.064
			2% Ag/ZrO_2	170		40.8	0.102

[a] See Table 1 for the BET surface area of catalysts.

[b] Measured amount of oxygen adsorbed divided by the amount of Ag in the sample.

[c] Calculated, assuming 2Ag:1O stoichiometry.

[d] Reduction extent, x, calculated after the oxygen adsorbed on silver (with 2Ag:1O stochiometry and assuming 100% silver dispersion) was subtracted from the actual amount of oxygen consumed.

[e] CeO_2 prepared by acetate decomposition at 750°C.

than 400°C (Fig. 9). The same is true for copper containing materials (Fig. 11). In both cases surface and bulk reduction cannot be separated, probably due to fast diffusion of the lattice oxygen to the surface. Our results indicate that the mechanism of methane oxidation over Ag-containing materials might be different and that it probably includes dissociative adsorption of oxygen and methane. XRD data (Fig. 6) show the presence of metallic Ag on Ag-modified catalysts. We may, then, surmise that CuO provides active oxygen for methane oxidation, while on Ag-modified catalysts, oxygen adsorbed on Ag must be active for methane oxidation.

Methane interacts mainly with the surface oxygen anions of ceria (coordinatively unsaturated oxygen (CUS) and lattice oxygen) (66). Since the interaction of methane with CUS oxygen is stronger than interaction with lattice oxygen (67), we presume that CUS species are responsible for methane activation on doped cerium oxide. Surface defects of ceria are sites for oxygen adsorption (67). Decrease of crystal size of ceria leads to the formation of surface defects and, therefore, a higher number of active sites. This is clearly demonstrated in Fig. 1 for undoped ceria. When heated to 750°C and 800°C, the crystal size of ceria grows to 20 nm and 24 nm, respectively, and the low temperature activity is lost. When the ceria crystal size is below 20 nm (650°C and 700°C treated ceria) the specific activity per surface area is about the same (Fig. 4, Table 3).

Generally, doping of CeO_2 leads to improved methane oxidation activity, as is clear from Fig. 4. Three different factors are considered to be important for the catalytic activity of doped ceria in redox reactions: crystal size, defect formation, and reducibility of surface oxygen species (30). Those factors are not independent. Doping of ceria leads to defect formation and in some cases to the reduction of the ceria crystal size. On the other hand, nanocrystalline materials are known to be highly defective (68). The reduction behavior of ceria depends on its surface area (surface oxygen reduction) and also on oxygen ion conductivity (bulk reduction). Both the surface and bulk reduction of ceria can be modified by doping.

The methane oxidation activity of doped CeO_2 catalysts can be related to the ability of surface oxygen to activate methane, leading to the removal of surface oxygen and to the ability of gas phase oxygen or bulk oxygen to fill a surface oxygen vacancy. Both La- and Zr-doped ceria show improved oxidation activity. One reason is the smaller grain size created by doping. Doping also changes the reduction properties of ceria. Both La and Zr improve the low-temperature reducibility of ceria (Table 4).

The activity of Zr-doped materials can be clearly attributed to the stabilization of small crystal size, and the consequent creation of surface defects. Zr as a tetravalent dopant does not create extrinsic oxygen vacancies. After high temperature treatment (800°C) the specific activity (rate per surface area) of Ce(10% Zr)O_2 decreases and approaches that of pure ceria. La-doped CeO_2 keeps its oxidation activity due to stabilized crystal size, as well as to the creation extrinsic oxygen vacancies. As Fig. 4 shows, the 10% La-doped ceria retained a much higher methane oxidation activity after the 800°C-treatment than the 10% Zr-doped ceria. The specific activity of La-doped ceria increases as La surface concentration increases (Fig. 4). The preexponential factors for methane oxidation over La-doped ceria are order of magnitude higher than those for undoped and Zr-doped ceria.

The effect of ceria crystal size on methane oxidation activity is evident. Enhanced reactivity of nanocrystalline ceria is in agreement with the results reported previously for CO oxidation. Tschöpe *et al*. (69) showed that nonstoichiometric nanocrystalline cerium oxide has a 200°C-lower light-off temperature for CO oxidation than precipitated stoichiometric CeO_2, presumably due to the rapid formation of adsorbed oxygen species (superoxide) on the former as a result of the presence of free electrons. It is known that superoxide species (O_2^-) are formed on a partially reduced CeO_2 surface (66,70). However, the nonstoichiometry of ceria has a much lower effect on the methane oxidation activity (44, 69) probably due to the higher temperatures needed for methane activation (>400°C). At such temperatures electrophilic oxygen species, such as the superoxide species, are quickly converted to lattice oxygen (66,70).

In the presence of a transition metal both ceria and the metal (Ag)/metal oxide (CuO) are active catalyst components. Addition of the transition metal clearly increases the reducibility of ceria at low temperatures, as is demonstrated here by H_2- and CH_4-TPR for copper-containing catalysts and by oxygen chemisorption for Ag-containing materials. On the other hand, ceria modifies the properties (dispersion, oxidation state, and reducibility (18,19,53,55)) of the supported metal/metal oxide. Strong interaction between Cu^{+1} clusters and CeO_2, results in enhanced activity for CO oxidation (44). In recent work, we reported on the reducibility and activity in the complete oxidation of methane of various copper species formed when copper oxide is supported on ceria and zirconia (53). Copper clusters, identified at low copper loading (5 at%) are less reducible than highly dispersed copper oxide particles (present at higher copper loading, 15 at%), when copper is supported on zirconia (53). Similar behavior was found for copper supported on ceria. However, copper species formed on zirconia reduce at lower temperature (both in H_2 and CH_4) rather than the corresponding copper species on ceria due to the strong interaction between ceria and CuO_x. When ceria is used as an active support, the properties of both ceria and the transition metal are modified so that their individual contributions to the overall methane oxidation activity cannot be separated. At low copper loading, the rate of methane

oxidation (expressed per gram or surface area of catalyst) is higher on ceria-supported copper catalysts than that on zirconia-supported materials (53). However, at higher copper loading, zirconia-supported catalysts are more active than the ceria-supported ones (53). This is attributed to lower reducibility of copper oxide species formed on zirconia.

Similar enhancement of the reducibility of ceria is reported here for ceria-supported silver. The promotion of ceria reducibility is a strong function of crystal size as the results in Table 5 indicate. Although the reasons for such behavior are not clear, this enhancement is probably the result of a defective structure of nanocrystalline ceria. Small crystals of ceria interact with Ag more strongly, so that the reactivity of ceria is enhanced. Addition of Ag to Ce-Al-O support was shown to enhance the formation of O_2^- (38). Previous reports show that introduction of noble metals (Pt, Pd) increases the reactivity of O_2^- species on ceria at low temperature (38,39). This is the type of oxygen that more likely participates in CO oxidation (55,71). The increased reducibility of the doped CeO_2 support leads to higher activity of the superoxide species so that the Ag-modified Ce(50% Zr)O_2 has the highest activity for CO oxidation. The same is true for methane oxidation, although at the higher temperature range of the latter, adsorbed oxygen species are quickly converted to lattice oxygen.

The availability of low temperature oxygen species on ceria is not the only important factor for methane oxidation over Ag-containing catalysts. Ag metal supported on an inert support is an active catalyst as the data of Fig. 4 clearly show. When Ag is supported on ceria, the contribution of Ag and ceria to the overall catalytic activity can not be separated. Ag promotes the ceria reducibility (Table 5). However, ceria-supported Ag catalysts with 5% Ag loading have lower activity then Ag/ZrO_2, although high oxygen uptake at low temperature was measured (e.g., on 5% Ag/Ce(50% Zr)O_2). These differences may be attributed to the effect of Ag particle size. In other work (54), we have found that the methane oxidation activity is a strong function of Ag particle size, when Ag is supported on an inert support (ZrO_2), as was previously demonstrated for Pd (8) and Pt (72). The turnover rate increases as the Ag particle size increases up to 10 nm (54). Further increase in the particle size does not affect the activity. The difference in the activity can be attributed to a different structure of small (5 nm) and large (10 nm) Ag particles (54). As the Ag loading increases, larger Ag particles are formed, which give rise to XRD reflections of metallic Ag. These Ag particles can be easily seen by HRTEM as is illustrated in Fig. 12 for 5% Ag/ZrO_2.

To eliminate the effect of ceria, Ag-supported on low-surface area ceria, CeO_2^*, with large crystal size (~20 nm) was studied. The properties of this ceria and of the 3.4% Ag/CeO_2^* (ceria prepared by acetate decomposition) are

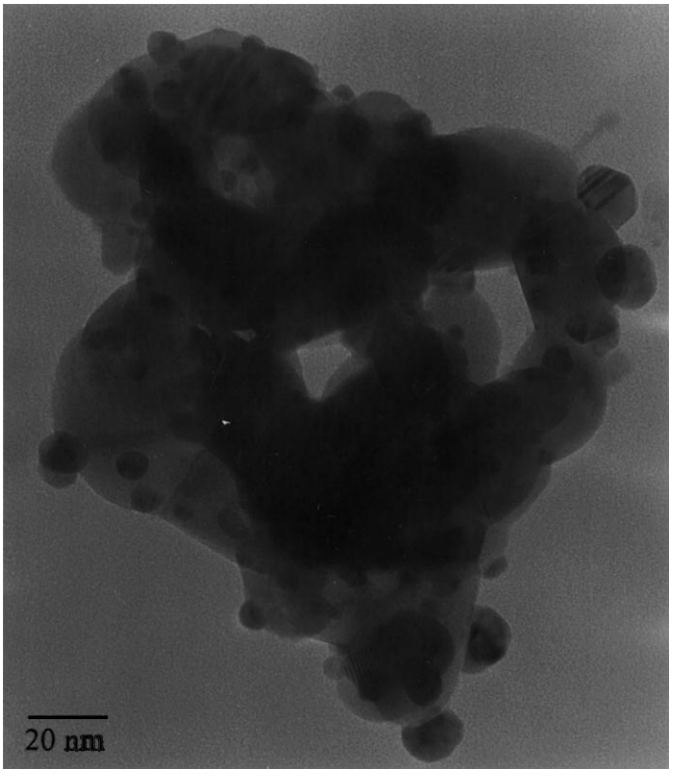

FIG. 12. HRTEM of 5% Ag/ZrO_2 catalyst.

listed in Table 1. The Ag-containing undoped ceria materials have low surface area, close to that of 3.5% Ag/ZrO_2 catalysts. The CeO_2^* material does not participate in the reaction as it was shown earlier (Fig. 1). The measured Ag dispersion in 3.4% Ag/CeO_2 is similar to that of 3.5% Ag/ZrO_2 materials at approximately the same Ag loading. However, the activity of Ag/ZrO_2 is much higher than that of Ag/CeO_2^*, as shown in Fig. 13.

For this 3.4% Ag/CeO_2^* catalyst, the silver particle size determined from oxygen chemisorption measurements, assuming that ceria does not contribute to the overall oxygen uptake, is much smaller (9.6 nm) than that measured by XRD (29.8 nm). This is attributed to nonuniform particle size distribution. When the sample consists of a large number of small crystallites and a small number of large crystallites, the width of the diffraction peak is determined mostly by the sharp peak of the larger crystallites. Ag/Ce(La,Zr)O_2 materials could not be analyzed by HRTEM due to the strong interaction of ceria with the electron beam. However, STEM/EDX analysis of Ce(La,Zr)O_2-supported Ag catalysts confirmed a nonuniform particle size distribution. Figure 14 shows elemental mappings of the 3.4 at% Ag/CeO_2^* catalyst. Ag-rich and ceria-rich regions were identified. In ceria-rich regions Ag appears to be uniformly dispersed. However, low Ag signal intensity indicates that only a small fraction of Ag is actually dispersed on ceria. The rest of Ag forms large (~400 nm) Ag particles. These large Ag

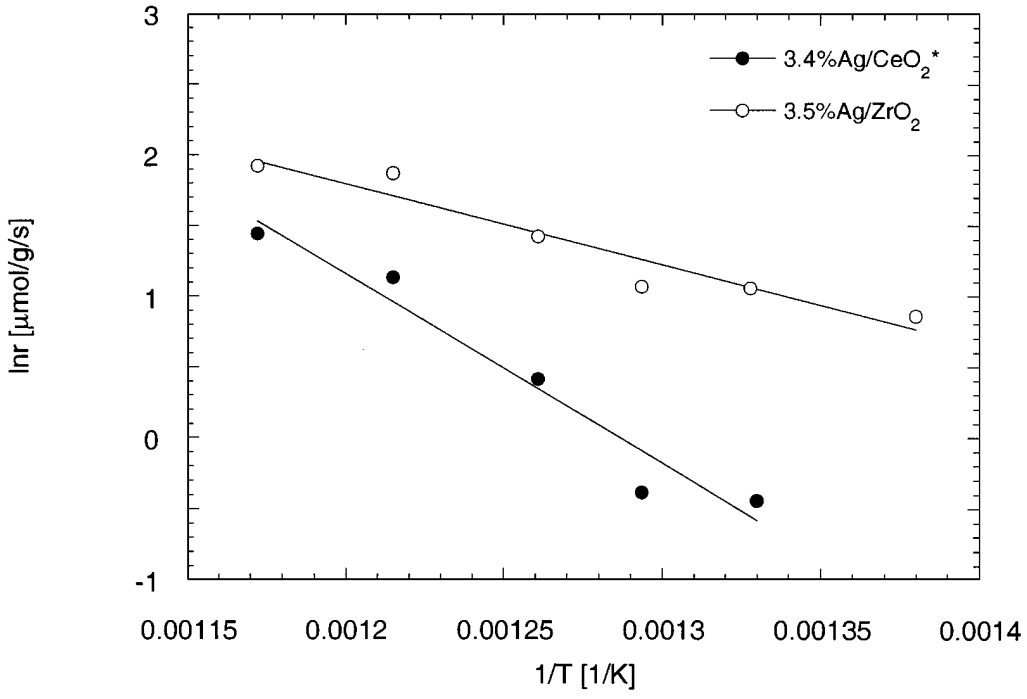

FIG. 13. Comparison of activity of 3.4% Ag/CeO_2^* (Table 1) and 3.5% Ag/ZrO_2 catalysts at the same Ag dispersion; 0.006–0.02 $g \cdot s/cm^3$ (STP), 1% CH_4, 5% O_2, balance He.

particles are covered by ceria and are not likely to participate in the reaction. Similar Ag distribution is observed for $Ag/Ce(La)O_2$ and $Ag/Ce(Zr)O_2$ catalysts. STEM analysis suggests that ceria-supported Ag materials contain only a small amount of highly dispersed silver and that most of the Ag is present as large (~400 nm) particles. Since the large Ag particles are covered by ceria, they are not the Ag active phase. The active phase comprises highly dispersed Ag clusters. Although the measured Ag dispersion is close to that of Ag/ZrO_2 materials with similar Ag content, the structure of supported silver on zirconia and ceria is different. Ceria as a support favors the formation of highly dispersed Ag clusters, while intermediate size Ag particles (~10 nm) which have the highest activity for methane oxidation (54) are not formed. The reasons for such behavior are not clear, but the predominance of highly dispersed Ag on ceria may explain their lower catalytic activity (Fig. 13).

CONCLUSIONS

Cu- and Ag-modified doped CeO_2 catalysts are active catalysts for the complete oxidation of methane. In the absence of the metal, doped CeO_2 is not inert. Rather, it provides sites for methane oxidation. The activity of methane oxidation on doped CeO_2 catalysts depends on surface oxygen availability. Loss of surface area and crystal size growth of ceria lead to lower methane oxidation activity. The sintering properties of ceria can be modified by doping. Dopants, such as La and Zr, decrease the ceria crystal size and prevent crystal growth at high temperatures, with concomitant higher methane oxidation activity. In addition, doping modifies both the surface and bulk reducibility of ceria. Both La- and Zr-doped materials are more reducible than undoped ceria. As a result, the methane oxidation activity is improved. Although Zr-doped catalysts have small crystal size and a large number of surface defects, doping of ceria with La which introduces extrinsic oxygen vacancies, further enhances the catalytic activity.

The addition of transition metals, such as Cu and Ag, improves the low-temperature CH_4 oxidation activity. The presence of the transition metal at low loading (<5 at%) enhances the reduction of the surface oxygen of ceria, as well as the ceria oxygen uptake. Oxygen reducibility and oxygen storage capacity seem to be important properties for the performance of ceria in oxidation reactions. Different oxygen species are present in mixed metal oxide catalysts as identified by TPR and chemisorption experiments: surface oxygen of the support and oxygen adsorbed on the transition metal (in the case of Ag-modified catalyst) or surface oxygen of the transition metal oxide (in the case of Cu-modified catalysts). Strong interaction between the transition metal and ceria, increases the ceria reducibility and its oxygen uptake. The oxygen uptake of Ag-modified catalysts clearly displays a synergism between the metal and the support. The oxygen uptake of the Ag-modified catalysts is higher than that of the nonmodified support. The

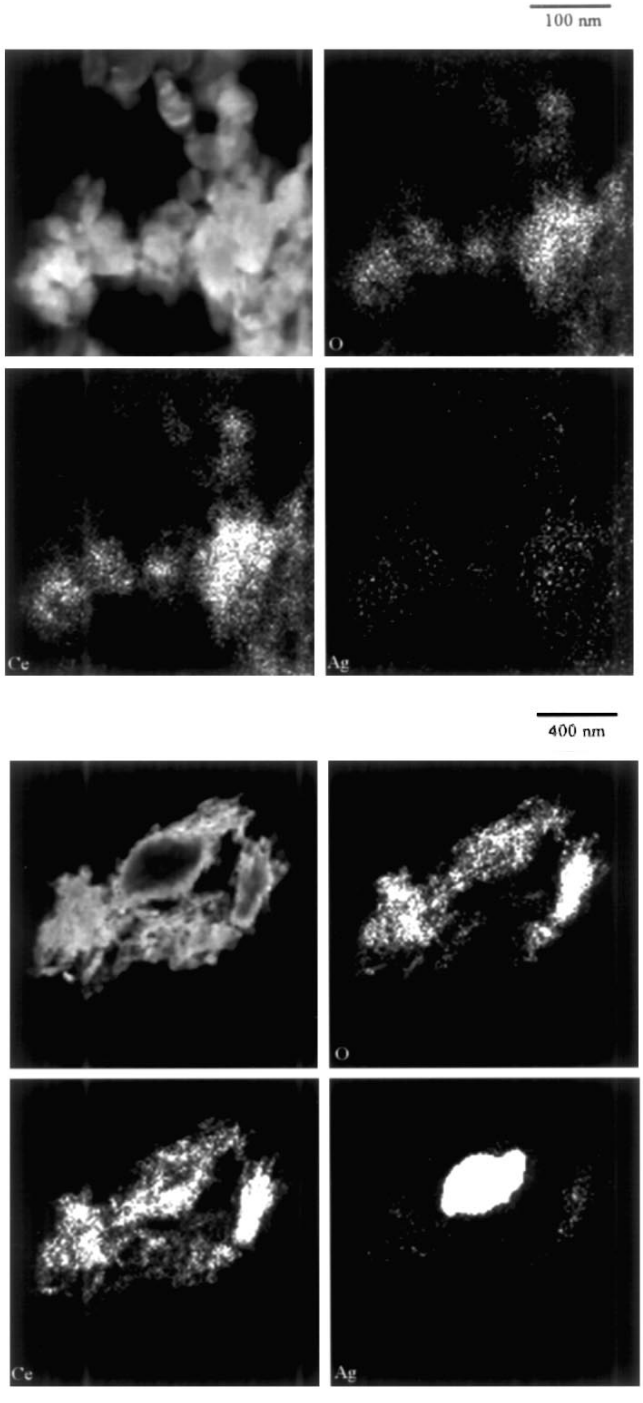

FIG. 14. STEM/EDX elemental mapping of 3.4% Ag/CeO_2 catalyst.

overall catalytic activity of ceria-supported CuO and Ag is influenced by both the ceria and the transition metal/metal oxide structure. A complex interaction between ceria and the transition metal/metal oxide modifies their properties and activity for methane oxidation.

REFERENCES

1. Lampert, J., Kazi, J. K., and Farrauto, R. J., *Appl. Catal. B: Environ.* **14**, 211 (1997).
2. Baldwin, T. R., and Burch, R., *Appl. Catal.* **66**, 337 (1990).
3. Baldwin, T. R., and Burch, R., *Appl. Catal.* **66**, 359 (1990).
4. Ribeiro, F. H., Chow, M., and Dalla Betta, R. A., *J. Catal.* **146**, 537 (1994).
5. Farrauto, R. J., Hobson, M. C., Kennelly, T., and Waterman, E. M., *Appl. Catal. A: General* **81**, 227 (1992).
6. Farrauto, R. J., Lampert, J. K., Hobson, M. C., and Waterman, M., *Appl. Catal. B: Environ.* **6**, 263 (1995).
7. Fujimoto, K., Ribeiro, F. H., Bell, A. T., and Iglesia, E., *in* "Symposium on Heterogeneous Hydrocarbon Oxidation, Division of Petroleum Chemistry, 211 National Meeting, American Chemical Society, New Orleans, LA, March, 1996," p. 110.
8. Fujimoto, K., Ribeiro, F. H., Iglesia, E., and Avalos-Borja, M., *in* "Symposium on Catalytic Combustion, Division of Petroleum Chemistry, Inc., 213 National Meeting, American Chemical Society, San Francisco, CA, April, 1997," p. 190.
9. Oh, S. H., Mitchell, P. J., and Siewert, R. M., *J. Catal.* **132**, 287 (1991).
10. Arai, H., Yamada, T., Eguchi, K., and Seiyama, T., *Appl. Catal.* **26**, 265 (1986).
11. McCarty, J. G., and Wise, H., *Catal. Today* **8**, 231 (1990).
12. Klvana, D., Vaillancourt, J., Kirchnerova, J., and Chaouki, J., *Appl. Catal. A: General* **109**, 181 (1994).
13. Kucherov, A. V., Slinkin, A. A., Goryashenko, S. S., and Slovetskaja, K. I., *J. Catal.* **118**, 459 (1989).
14. Kucherov, A. V., Kucherova, T. N., and Slinkin, A. A., *Kinet. Katal.* **33**(3), 618 (1992).
15. Ishihara, T., Sumi, H., and Takita, Y., *Chem. Lett.*, 1499 (1994).
16. Li, Y., and Armor, J. N., *Appl. Catal. B: Environ.* **3**, 275 (1994).
17. Anderson, R. B., Stein, K. C., Feenan, J. J., and Hofer, L. J., *Ind. Eng. Chem.* **53**, 809 (1961).
18. Liu, W., and Flytzani-Stephanopoulos, M., *J. Catal.* **153**, 304 (1995).
19. Liu, W., and Flytzani-Stephanopoulos, M., *J. Catal.* **153**, 317 (1995).
20. Liu, W., Sarofim, A. F., and Flytzani-Stephanopoulos, M., *Appl. Catal. B: Environ.* **4**, 167 (1994).
21. Liu, W., Wadia, C., and Flytzani-Stephanopoulos, M., *Catal. Today* **28**, 391 (1996).
22. Meriani, S., *Mater. Sci. Eng. A* **109**, 121 (1989).
23. Balducci, G., Fornasiero, P., Di Monte, R., Kaspar, J., Meriani, S., and Graziani, M., *Catal. Lett.* **33**, 193 (1995).
24. De Leitenburg, C., Trovarelli, A., Zamar, F., Maschio, S., Dolcetti, G., and Llorca, J., *J. Chem. Soc., Chem. Commun.*, 2181 (1995).
25. De Leitenburg, C., Trovarelli, A., Llorca, J., Cavani, F., and Bini, G., *Appl. Catal. A: General* **139**, 161 (1995).
26. Trovarelli, Q., Dolcetti, G. De Leitenburg, C., Kaspar, J., Finetti, P., and Santoni, A., *J. Chem. Soc. Faraday Trans.* **88**, 1311 (1992).
27. Tuller, H. L., and Nowick, A. S., *J. Electochem. Soc.* **2**, 255 (1975).
28. Inaba, H., and Tagawa, H., *Solid State Ionics* **83**, 1 (1996).
29. Harrison, B., Diwell, A. F., and Hallet, C., *Platinum Metals Rev.* **32**(2), 73 (1988).
30. Trovarelli, A., *Catal. Rev.-Sci. Eng.* **38**(4), 439 (1996).
31. Fornasiero, P., Di Monte, R., Ranga Rao, G., Kaspar, L., Meriani, S., Trovarelli, A., and Graziani, M., *J. Catal.* **151**, 168 (1995).
32. Zamar, F., Trovarelli, A., De Leitenburg, C., and Dolcetti, G., *J. Chem. Soc., Chem. Commun.* **9**, 965 (1995).
33. Zafiris, G. S., and Gorte, R. J., *J. Catal.* **139**, 561 (1993).
34. Cordatos, H., and Gorte, R. J., *J. Catal.* **159**, 112 (1996).
35. Cordatos, H., Bunluesin, T., Stubenrauch, J., Vohs, J. M., and Gorte, R. J., *J. Phys. Chem.* **100**, 785 (1996).
36. Putna, E. S., Vohs, J. M., and Gorte, R. J., *J. Phys. Chem.* **100**, 17862 (1996).

37. Bunluesin, T., Gorte, R. J., and Graham, G. W., *Appl. Catal. B: Environ.* **339**, 1 (1997).
38. Tarasov, A. L., Przheval'skaya, L. K., Shvets, V. A., and Kazanskii, V. B., *Kinet. Katal.* **29**(5), 1181 (1988).
39. Li, C., Chen, Y., Li, W., and Xin, Q., *in* "New Aspects of Spillover in Catalysis" (T. Inui *et al.*, Eds.), p. 217. Elsevier Science, Amsterdam, 1993.
40. Yao, H. C., and Yao, Y. F. Y., *J. Catal.* **86**, 254 (1984).
41. Nunan, J. G., Silver, R. G., and Bradley, S. A., *in* "Catalytic Control of Air Pollution" (R. G. Silver, J. E. Saeyer, and J. C. Summers, Eds.), Chap. 17. ACS Symposium Series, Vol. 495, Am. Chem. Soc., Washington, DC, 1992.
42. Aboukais, A., Bennani, A., Aissi, C. F., Guelton, M., and Vedrine, J. C., *Chem. Mater.* **4**, 977 (1992).
43. Soria, J., Conesa, J. C., Martinez-Arias, A., and Coronado, J. M., *Solid State Ionics* **63–65**, 755 (1993).
44. Liu, W., "Development of Novel Metal Oxide Composite Catalysts for Complete Oxidation Reactions," Sc.D. thesis, MIT, 1995.
45. Amenomiya, Y., Emesh, A., Oliver, K., and Pleizer, G., *in* "Proc. 9th Intern. Cong. Catal." (M. Phillips and M. Ternan, Eds.), p. 634. Chemical Inst. of Canada, Ottawa, Canada, 1988.
46. Pijolat, M., Prin, M., Soustelle, M., Touret, O., and Nortier, P., *Solid State Ionics* **63–65**, 781 (1993).
47. Pijolat, M., Prin, M., Soustelle, M., Touret, O., and Nortier, P., *J. Chem. Soc. Faraday Trans.* **91**(21), 3941 (1995).
48. Pal'guev, S. F., Alyamosvkii, S. I., and Volchenkova, Z. S., *Russ. J. Inorg. Chem.* **4**, 1185 (1959).
49. Meriani, S., *Mater. Sci. Eng.* **71**, 369 (1985).
50. Meriani, S., and Spinolo, G., *Powder Diffraction* **2**(4), 255 (1987).
51. Yashima, M., Morimoto, K., Ishizawa, N., and Yoshimura, M., *J. Am. Cer. Soc.* **76**(7), 1745 (1993).
52. Yashima, M., Arashi, H., Kakihana, M., and Yoshimura, M., *J. Am. Cer. Soc.* **77**(4), 1067 (1994).
53. Kundakovic, Lj., and Flytzani-Stephanopoulos, M., *Appl. Catal. A: General* **171**(1), 13 (1998).
54. Kundakovic, Lj., and Flytzani-Stephanopoulos, M., *Appl. Catal. A: General*, submitted.
55. Kundakovic, Lj., Ph.D. thesis, Tufts University, 1998.
56. Johnson, F. L., and Mooi, J., *J. Catal.* **140**, 612 (1987).
57. Laachir, A., Perrichon, V., Badri, A., Lamotte, J., Catherine, E., Lavalley, J. C., El Fallah, J., Hilaire, L., Le Normand, F., Quemere, E., Sauvion, G. N., and Touret, O., *J. Chem. Soc. Faraday Trans.* **87**(10), 1601 (1991).
58. Zotin, F. M. Z., *J. Catal.* **98**, 99 (1993).
59. Perrichon, V., Laachir, A., Bergeret, G., Frety, R., Tournayan, L., and Touret, O., *J. Chem. Soc. Faraday Trans.* **90**, 773 (1994).
60. Bernal, S., Calvino, J. J., Cifredo, G. A., Gatica, J. M., Perez-Omil, J. A., and Pintando, J. M., *J. Chem. Soc. Faraday Trans.* **89**, 3499 (1993).
61. Bernal, S., Botana, F. J., Calvino, J. J., Cauqui, M. A., Cifredo, G. A., Jobacho, J., Pintado, J. M., and Rodriguez-Izquierdo, J. M., *J. Phys. Chem.* **97**, 4118 (1993).
62. Binet, C., Badri, A., and Lavalley, J.-C., *J. Phys. Chem.* **98**, 6392 (1994).
63. Fierro, G., Jacono, M. L., Inversi, M., Porta, P., Lavecchia, R., and Cioci, F., *J. Catal.* **148**, 709 (1994).
64. Liu, W., and Flytzani-Stephanopoulos, M., *Chem. Eng. J.* **64**, 283 (1996).
65. Smeltzer, W. W., Tollefson, E. L., and Cambron, A., *Can. J. Chem.* **34**, (1956).
66. Li, C., and Xin, Q., *J. Phys. Chem.* **96**, 7714 (1992).
67. Li, C., Domen, K., Maruya, K., and Onishi, T., *J. Am. Chem. Soc.* **111**, 7683 (1989).
68. Zhang, Y., Andersson, S., and Muhammed, M., *Appl. Catal. B: Environ.* **6**, 325 (1995).
69. Tschope, A., Liu, W., Flytzani-Stephanopoulos, and Ying, J. Y., *J. Catal.* **157**, 42 (1995).
70. Zhang, X., and Klabunde, K. J., *Inorg. Chem.* **31**, 1706 (1992).
71. Sass, A. S., Shvets, V. A., Savel'eva, G. A., Popova, N. M., and Kazanskii, V. B., *Kinet. Katal.* **27**(4), 894 (1986).
72. Otto, K., *Langmuir* **5**, 1364 (1989).